

# Unsteady waves generated by a ship travelling over a step bottom

Mingxin Li<sup>1,2</sup>, Zhi-Ming Yuan<sup>1\*</sup>, and Ronald W. Yeung<sup>3</sup>

<sup>1</sup> Dep. of Naval Architecture, Ocean & Marine Engineering, University of Strathclyde, UK

<sup>2</sup> School of Naval Architecture and Ocean Engineering, Jiangsu University of Science and Technology, Zhenjiang, China

<sup>3</sup> Department of Mechanical Engineering, University of California at Berkeley, CA 94720, USA

\*E-mail address of the presenting author: [zhiming.yuan@strath.ac.uk](mailto:zhiming.yuan@strath.ac.uk)

## HIGHLIGHTS

- The unsteady ship waves excited by passing an abrupt change in bottom depth are presented.
- A periodic oscillation of the wave-making resistance is observed after such an excitation.

## INTRODUCTION

Although ships do spend the majority of their operational time sailing at waterways of uniform depth, there are circumstances when the unsteady effects can be important. Among these examples are:

- 1) In practical operations when a ship manoeuvres in a port/harbour/lock environment. Under this circumstance, a ship is likely to travel in close proximity to waterway boundaries that have abrupt change, i.e. a step change in bank dimension or bottom depth;
- 2) During ship model testing, a false bottom has been considered to be installed to mimic the change of the water depth in an "idealistic" way. Such false bottom usually does not cover a full length of the towing tank. Therefore, as a ship model manoeuvres from deep water to finite-depth water, unsteady effects will be experienced;
- 3) When conducting ship model tests in a towing tank, the ship model is accelerated from the rest to the target speed. The measured resistance was found to experience persistent periodic oscillations after the target speed was achieved (Doctors, Day et al. 2008).

The aforementioned unsteady circumstances have received only limited amount of attention. The first two situations involve changing boundary shapes in time, when viewed from the ship-fixed coordinate system, which requires tremendous computational efforts of meshing. In the third situation, although the physical boundaries are not changing, the body surface boundary condition is unsteady because of the time-dependent ship speed. The expected behaviour of this solution within the context of linear theory was discussed in the seminal work of Wehausen (1964), with experimental results by Calisal (1977) and lately Doctors et al. (2008). However, the first two circumstances, which are related, have been less well studied, with the exception of Alam & Mei (2008), particularly the interesting unsteady three-dimensional wave fields. This presentation will address these two situations, especially focusing on the unsteady waves generated by a ship moving over a step bottom. The wave field behaviour, even though three-dimensional, is now more amenable to expedient numerical treatment with the use of Green's theorem for the full fluid domain (see Yeung, 1982; Kring, 1994).

## INITIAL BOUNDARY-VALUE PROBLEM (BVP)

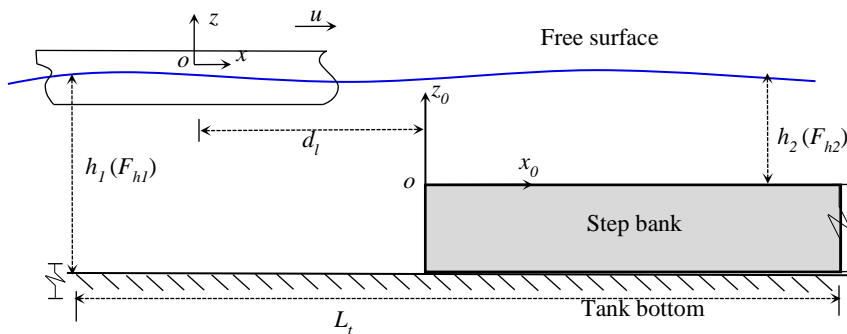


Figure 1. The sketch of the problem and the definition of the coordinate systems.

Two right-handed coordinate systems are used: a global reference frame  $O-x_0y_0z_0$  fixed to the leading corner of the step bottom, and a local reference frame  $o-xyz$  fixed to the body, as shown in **Figure 1**. Within the framework of potential-flow theory, which neglects the viscosity and compressibility of the fluid, the motion can be described by a disturbance velocity potential  $\varphi(x,y,z,t)$ , which satisfies the Laplace equation in the field. On the body surface, sea bottom and control surfaces, the same boundary conditions as used in the steady-state problem (Yuan, Li et al. 2019) are applied in the present study. In order to account for the unsteady effect, the unsteady nonlinear free surface condition are applied. The unsteady nonlinear kinematic and dynamic free surface condition can be written as following

$$\zeta_t - u\zeta_x + \varphi_x\zeta_y + \varphi_y\zeta_x - \varphi_z = 0, \text{ on } z = \zeta \quad (1)$$

$$\varphi_t + g\zeta - u\varphi_x + \frac{1}{2}\left[(\varphi_x \cdot \varphi_x) + (\varphi_y \cdot \varphi_y) + (\varphi_z \cdot \varphi_z)\right] = 0, \text{ on } z = \zeta \quad (2)$$

where  $\zeta(x, y, t)$  is the free surface elevation and  $g$  is the gravitational acceleration. The free surface condition is satisfied on the unknown surface  $z = \zeta$ .

An iterative algorithm with implicit finite-difference scheme is developed to solve this unsteady nonlinear BVP. The nonlinear equation (1) and (2) is of fully implicit type. The solution of these two equations can be obtained iteratively. The initial value of the variables  $\varphi$  and  $\zeta$  at the time  $t = 0$ , are given by the solutions of the steady-state Neumann-Kelvin problem. At  $t = 0$ , the time-dependent non-linearized free surface condition in equations (1) and (2) are reduced to the linearized free surface condition given as:

$$u^2\varphi_{xx} + g\varphi_z = 0, \text{ on } z = 0 \text{ at } t = 0 \quad (3)$$

The time derivatives in the free surface condition have to be discretized. A three-time-level scheme is used to obtain the first derivatives of  $\varphi$  and  $\zeta$ .

$$(\varphi_t)_{i,j}^{n+1} = \frac{1}{\Delta t} \left( \frac{3}{2}\varphi_{i,j}^{n+1} - 2\varphi_{i,j}^n + \frac{1}{2}\varphi_{i,j}^{n-1} \right), \quad (\zeta_t)_{i,j}^{n+1} = \frac{1}{\Delta t} \left( \frac{3}{2}\zeta_{i,j}^{n+1} - 2\zeta_{i,j}^n + \frac{1}{2}\zeta_{i,j}^{n-1} \right) \quad (4a,b)$$

where the subscripts  $i, j$  indicate the indices of the longitudinal and transverse panel number respectively on the free surface rectangular mesh. At each iterative step  $k$ , the linear terms of the  $x$ -derivatives in (1) are approximated implicitly on the left-hand side (LHS) terms. The cross-derivatives and the rest of the nonlinear terms are put on the right-hand sides (RHS) as the known for the next iteration at  $t = t_{n+1}$  to update the wave elevation. The dynamic condition in (2) is then satisfied through an implicit method using the solutions at  $t_n$  to update potential  $\varphi$  at  $t_{n+1}$ . All variables are then updated by the latest values from the iteration as  $k$  is advanced. Thus, at each iterative step  $k$ , (4a) and (4b) can be written as (5) and (6) below, respectively:

$$\frac{3\zeta_{i,j}^{n+1,k} - 4\zeta_{i,j}^n + \zeta_{i,j}^{n-1}}{2\Delta t} - u \cdot (\zeta_x)_{i,j}^{n+1,k} = -(\varphi_x)_{i,j}^n \cdot (\zeta_x)_{i,j}^n - (\varphi_y)_{i,j}^n \cdot (\zeta_y)_{i,j}^n + (\varphi_z)_{i,j}^n \quad (5)$$

$$\frac{3\varphi_{i,j}^{n+1,k} - 4\varphi_{i,j}^n + \varphi_{i,j}^{n-1}}{2\Delta t} - u \cdot (\varphi_x)_{i,j}^{n+1,k} = -g \cdot \zeta_{i,j}^{n+1,k} - \frac{1}{2} \left[ (\varphi_x \cdot \varphi_x)_{i,j}^{n,k} + (\varphi_y \cdot \varphi_y)_{i,j}^{n,k} + (\varphi_z \cdot \varphi_z)_{i,j}^{n,k} \right] \quad (6)$$

In the above,  $\varphi_{i,j}^{n+1,k}$  and  $\zeta_{i,j}^{n+1,k}$  are the predicted values of  $\varphi_{i,j}^{n,k}$  and  $\zeta_{i,j}^{n,k}$  after the  $k$ th iteration. In order to obtain more stable numerical results, a 2<sup>nd</sup>-order up-wind difference scheme was implemented to obtain the spatial derivatives of  $\varphi_x$  and  $\zeta_x$  on the LHS of the (5) and (6) (Kring 1994). The transverse derivatives and the vertical derivatives of the nonlinear items are evaluated by using a central difference scheme. The implicit scheme is unconditionally stable and its temporal and spatial accuracy is of second order, i.e.  $O(\Delta t^2)$ ,  $O(\Delta x^2, \Delta y^2)$ .

Once the unknown potential  $\varphi$  is solved at the  $(x_i, y_j)$  grid point, the time-dependent wave-making resistance can be obtained by pressure integral over the hull surface  $S$

$$R_w = -\iint_S p n_x dS = \iint_S \rho \left( \varphi_t - u\varphi_x + \frac{1}{2} \left[ (\varphi_x \cdot \varphi_x) + (\varphi_y \cdot \varphi_y) + (\varphi_z \cdot \varphi_z) \right] \right) n_x dS \quad (7)$$

It should be noted that a negative  $R_w$  indicates the force acting against the direction of ship movement. The wave elevation on the free surface can be obtained from the dynamic free surface boundary condition in (2) in the following form:

$$\zeta(x, y, t) = -\frac{1}{g} \left( \varphi_t - u\varphi_x + \frac{1}{2} \left[ (\varphi_x \cdot \varphi_x) + (\varphi_y \cdot \varphi_y) + (\varphi_z \cdot \varphi_z) \right] \right) \quad (8)$$

## RESULTS AND DISCUSSIONS

**Figure 2** shows the wave patterns by a moving single source point of unit source density. The analytical solution of the linear steady-state wave patterns by Peters (1949) is used here to validate the present calculations, as shown in **Figure 2 (a)**. Generally, with careful numerics, this type of Rankine source (or "Simple-source," per Yeung, 1982) panel method provides good agreement with the analytical solutions. As the waves propagate to the far field downstream, a phase shift gradually appears, which is caused by the numerical dispersion and dissipation of the algorithm. A comparison between the waves in deep water and that in shallow water, as shown in **Figure 2 (b)** and (c), shows that both the wave length and amplitude are different. An interesting question thus arises: what are the waves generated by a source point moving from deep water to shallow water as in the case of passing over a step bottom? One can imagine that the waves will eventually approach those of the steady shallow-water waves when the transit time is long enough. But before the waves reach a new steady phase, they must experience a transition phase which is oscillatory in time. In the present work, we are interested in this unsteady, transition phase and will examine how the deep water waves developed differently into the shallow water waves.

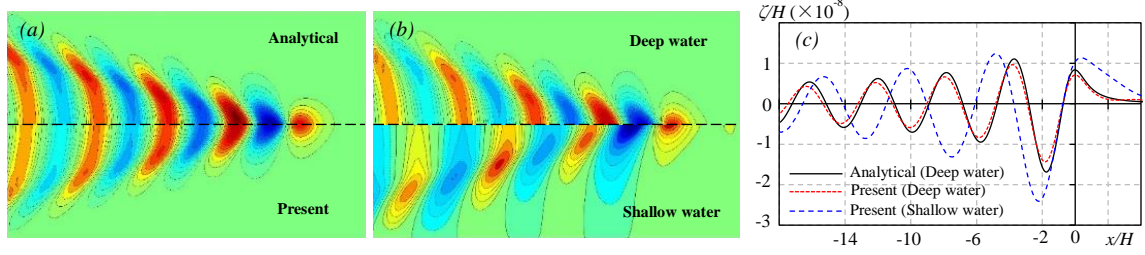


**Figure 2.** The steady waves generated by a moving source point ( $F_n = u / \sqrt{gH} = 0.8$ ) submerged at a depth of  $H$ , taken as  $1/4$  steady wavelength, i.e.  $H=0.5\pi u^2/g$ . (a) Comparison of deep water wave pattern between analytical solution and the present calculations. The horizontal and transverse axes are given by  $x/H$  and  $y/H$  respectively; (b) Comparison of the wave patterns in deep water and shallow water (The water depth is  $h = 1.05*H$  and the depth Froude number is  $F_h = 0.78$  ( $F_h = u / \sqrt{gh}$ )); (c) Comparison of the wave profile at the centerline:  $y=0$ .

**Figure 3** shows the time history of the pressure acting on a source point when it passes over a step bottom of different depths. Before the source point reaches the leading edge of the step bottom, the pressure is nearly steady. After that, interestingly, this pressure starts to oscillate almost periodically. The oscillation of the pressure persists for a long time before it decays to a steady-state value, which corresponds to the steady pressure on the source moving in constant-depth shallow water. From a separate analysis (Li et al, 2020), one can show the appropriate normalized time scale to be used is  $tg/(\delta\pi)u$ . The amplitude and the period of the oscillation is highly dependent on the water-depth ratio at the step bottom: a shallower water depth will induce an oscillation of larger amplitude and longer period, and vice versa.

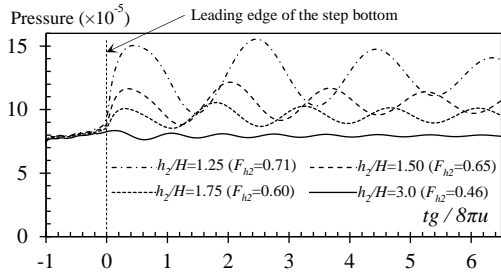


**Figure 3.** Time histories of the (non-dimensional) pressure ( $p/\rho u^2$ /source strength) at  $(x, y, z)=(0, 0, 0)$  when it moves from deep to shallow water (passing over a step bottom).  $H$  is the submerged depth of the source point, defined in **Figure 2** and  $h_2$  is the water depth at the step bottom.  $t=0$  corresponds to the instant when the source point reaches the leading edge of the step bottom.

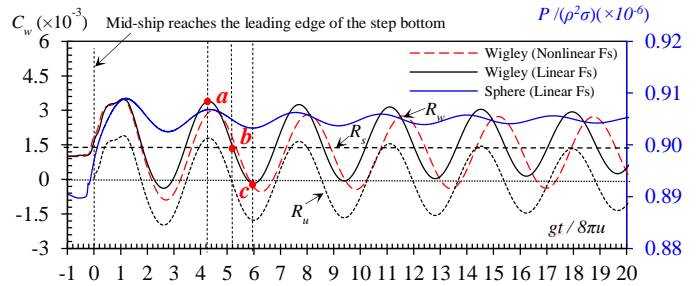


**Figure 4.** Time histories of the wave-making resistance coefficient ( $C_w = R_w / (1/2 \rho u^2 S)$ , where  $\rho$  is the water density and  $S$  is the wetted surface area of the hull) of a Wigley III hull passing over a step bottom from  $F_{h1}=0.3$  to  $F_{h2}=0.85$ . The total resistance time-dependent  $R_w$  is the sum of the steady resistance  $R_s$  and unsteady resistance  $R_u$ . The blue curve is the average non-dimensional pressure on a very small sphere ( $R/H=0.2$ ) submerged at  $H=0.25\pi u^2/g$ , travelling from  $F_{h1}=0.3$  to  $F_{h2}=0.85$ .

Replacing the source point with a ship hull, which is of more practical interest, one can obtain the time history of the wave-making resistance by pressure integral of (7). Similar oscillation phenomenon is observed, as shown in **Figure 4**. The wave-making resistance oscillates periodically around a mean steady resistance. A decay of the oscillation amplitude can be found. Obviously, the oscillation decays very slowly, indicating the oscillation will be eventually vanished only if the time is sufficiently large. To quantify the unsteady effects, we separate the unsteady component  $R_u$  and  $\zeta_u$  from the total wave-making resistance and wave elevation as

$$R_u = R_w - R_s, \quad \zeta_u = \zeta - \zeta_s \quad (9a, b)$$

where  $R_w$  and  $\zeta$  is the total wave-making resistance calculated by solving the unsteady BVP.  $R_s$  and  $\zeta_s$  are the corresponding quantities for the steady solution obtained by solving the steady-state BVP. As shown in **Figure 4**, the fluctuation of the unsteady wave-making resistance component in the first three oscillations is factually larger than the mean steady component, which should attract particular attention in practical manoeuvres. Of interest, we find some negative wave-making resistance momentarily (acting in the same direction of ship movement) after the ship passes the leading edge of the step bottom, e.g. at the time instants of  $tg/8\pi u=2.8$  and  $6.0$ .

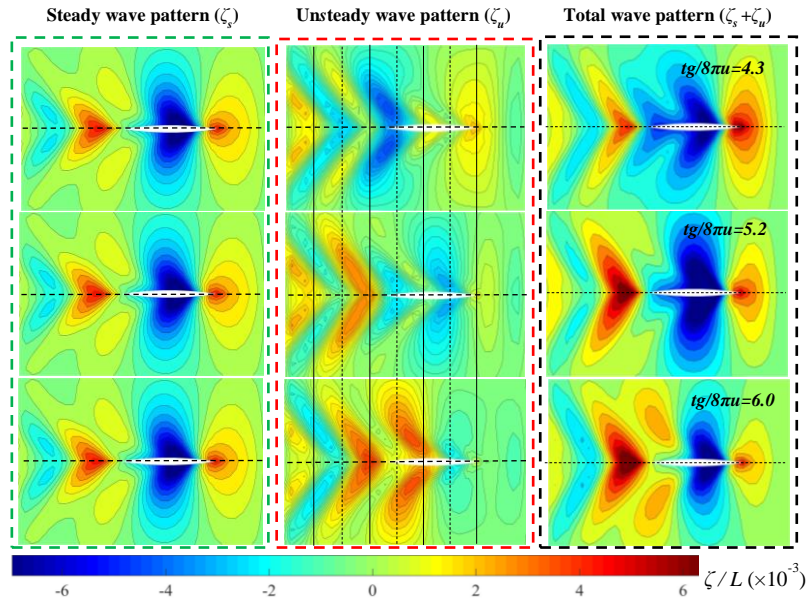


**Figure 5.** The steady and unsteady transient wave contour at three selected positions. The first column presents the steady wave pattern generated by the Wigley III ship model at  $F_n = 0.3$  and  $H/D = 2$  ( $F_h = 0.85$ ). The middle column shows the unsteady wave pattern, and the third column shows the sum of the first two columns (as defined by Eqn. (9b)).

The periodic oscillation of the wave-making resistance is significantly correlated with the unsteady waves. As the resistance curve in **Figure 4** is near-harmonic, it would be interesting to investigate the evolution of the unsteady waves in one half period, i.e. from  $tg/8\pi u=4.3$  to  $6.0$ . Three typical points are highlighted: "a",  $tg/8\pi u=4.3$ , where the maximum unsteady wave-making resistance is found; "b",  $tg/8\pi u=5.2$ , where the unsteady wave-making resistance is zero (the total wave-making resistance is the same as the steady component); "c",  $tg/8\pi u=6.0$ , where the minimum unsteady wave-making resistance is observed. **Figure 5** shows the wave contour at these three points. The unsteady wave component  $\zeta_u$  presents similar patterns as steady Kelvin waves. Under body-fixed coordinate system, the phase of the wave remains unchanged, but the elevation is subject to a periodic change. Let's take the wave crest at ship bow as an example. At these three points, it is always crest. However, the elevation experiences a reduction from maximum to zero. Due to the change of the elevation, the pressure distribution at these three instants in time are different. At *a*, a high pressure is distributed over the ship bow area, while a low pressure is distributed over the ship stern area. It is in phase with the steady pressure. The total wave elevation is amplified because of the constructive interference between the steady and unsteady waves, and the total wave-making resistance has therefore reached its maximum by the superposition of the steady and unsteady components. As the time moves forward to point *c*, the situation is reversed. At this moment, the transient unsteady waves are out of phase with the steady waves. Owing to the destructive wave interference, a minimum wave-making resistance can result. Particularly, at point *b*, the unsteady pressure distributed over the stern and bow is in balance, consequently, the unsteady wave-making resistance at this position is zero. In short, the oscillation of the wave-making resistance can be explained by the interference between the steady and unsteady waves at the bow and stern locations.

## REFERENCES

- Alam, M.-R. and C. C. Mei (2008). *Journal of Fluid Mechanics* **616**: 397-417.  
 Calisal, S., J. Ship Res. 21, 4, 239-247  
 Doctors, L. J., A. H. Day and D. Clelland (2008). *Journal of Ship Research* **52**(4): 263-273.  
 Kring, D. C. (1994). "Time domain ship motions by a three-dimensional Rankine panel method." Univ Michigan, *PhD Thesis*.  
 Peters, A. S. (1949). *Communications on pure and applied mathematics* **2**(2 - 3): 123-148.  
 Yeung, R. W. (1982). *Ann. Review of Fluid Mech.*, vol. 14, pp.395-442.  
 Yuan, Z. M., M. Li, C. Y. Ji, L. Li, L. Jia and A. Incecik (2019). *J R Soc Interface* **16**(150): 20180768.  
 Li, M., Z.-M. Yuan and R. W. Yeung (2020) OMAE-2020 Conference, Paper # 19350, June 28-July 3, 2020  
 Wehausen, J. V. (1964), *J. Ship Res.* 1, 38-50